Implementation & Design of Physical Radar Waveform Diversity

John Jakabosky, *IEEE Graduate Student Member,* Patrick McCormick, *IEEE Graduate Student Member*, Shannon D. Blunt, *IEEE Fellow*

The authors are with the Electrical Engineering & Computer Science Dept., Radar Systems & Remote Sensing Lab, University of Kansas, Lawrence, KS.

I. INTRODUCTION

Echo-locating mammals have been exploiting waveform diversity (WD) for about 50 million years [1], and the notion of radar waveform design has been around for several decades (see [2] and references therein). However, the current instantiation of WD was first popularized in 2002 in the hopes of addressing the growing competition for radar spectrum [3]. Since that time, there has been a tremendous amount of work on myriad aspects of WD (e.g. [4]), with a particular emphasis on leveraging higher dimensionality (e.g. multiple-input multiple-output, or MIMO). Much of this work has focused on the complex mathematical modeling and subsequent optimization of radar "waveforms" (noting that the term tends to be used rather loosely). Here we summarize recent work that seeks to connect the parameterized mathematical abstraction of radar codes, which provide the benefit of being readily optimizable, with the physical attributes and limitations of real radar systems and phenomenology. This physical perspective permits realization of the promised performance enhancements of WD on actual hardware, as well as providing the means with which to address radar spectrum issues for real systems.

Fundamentally, a radar waveform is a modulation of the transmitted signal in such a way that, when the received echoes are match filtered (or at least minimally mismatched) to the waveform, a processing gain is achieved that helps to separate the echoes from noise and to distinguish the echoes from one another. This process is generally known as "pulse compression" and decades of contributions have included a litany of waveform and filter design approaches [2].

Phase coding is one way in which to modulate the transmitted signal and includes numerous contributions such as Barker codes, P-codes, minimum peak sidelobe (MPS) codes, and many others (see [2, Chap. 6]). The code structure, comprised of rectangular chips (or sub-pulses) modulated by the phase values of the code, provides a convenient framework for design (Fig. 1). However, this idealized mathematical representation possesses extended spectral sidelobes having a $\sin(x)/x$ envelope due to instantaneous phase transitions [2, pp. 145-155].
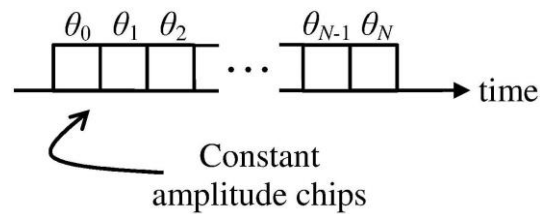

Figure 1: Idealistic representation of phase-coded modulation of the transmit signal

Figure 2 illustrates the distortion that occurs when such a code (here a P4 code [2]) is loaded onto an arbitrary waveform generator (AWG), injected into a S-band transmitter using a class AB solid-state GaN power amplifier, and then directly captured by a receiver in a loopback configuration (i.e. no free space transmission). It is observed that the intrinsic bandlimiting and nonlinear distortion of the transmitter (particularly the power amplifier) have significantly curtailed the spectral spreading of the original signal. While this result may appear to have positively addressed the spectral containment problem, the associated mismatch is actually a loss in fidelity that can limit performance in the radar receiver [5].
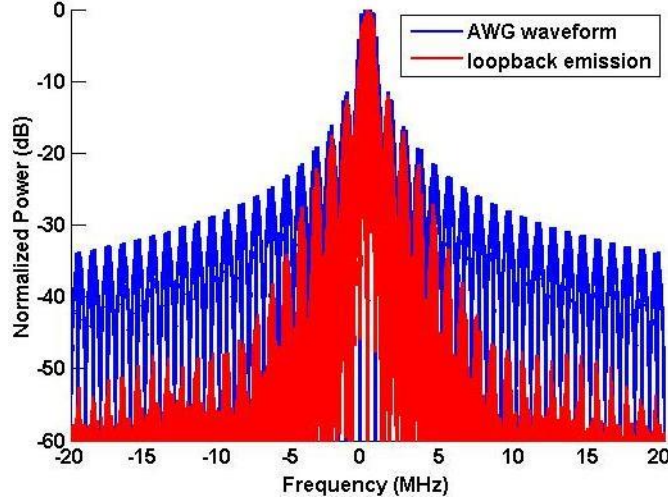
Figure 2: Spectral content of phase-coded modulation before and after the transmitter [6]

As elaborated in [6], it is thus useful to clarify the distinction between the terms *code*, *waveform*, and *emission*. The *code* consists of a finite set of sequential phase values $[\theta_0, \cdots, \theta_N]$ pertaining to some implementation structure (e.g. idealistic rectangular chips). In contrast, the *waveform* is a continuous modulating signal whose spectral content is relatively amenable to the natural bandlimiting imposed by the transmitter. Perhaps the most well-known waveform is the linear frequency modulated (LFM) chirp [2, pp. 57-61], along with many variants of nonlinear FM waveforms (e.g. [7-12]). Finally, the *emission* is defined as the physical signal launched into free space by the radar, inclusive of transmitter distortion effects, non-instantaneous pulse rise/fall-times (if pulsed), and electromagnetic coupling effects from the antenna and radar platform (this effect is most pronounced for MIMO emissions [13]).

To achieve the promised sensing enhancements and spectral containment of WD, one must consider the physical emission launched from the radar. Further, to achieve the benefits of optimal/adaptive waveform-domain receive processing necessitates sufficient fidelity [14,15] that can only be obtained by leveraging a loopback capture of the physical emission. The following describes an implementation of polyphase codes as transmitter-amenable waveforms based on the continuous phase modulation (CPM) scheme previously used in communications [16]. The

resulting polyphase-coded FM (PCFM) waveforms [6] are readily implementable on high-power radar systems, yet can be optimized like codes [14]. By extension, this same framework permits inclusion of transmitter distortion so as ultimately to enable optimization of the free space radar emission [14]. Recent work on the extension to fast-time polarization modulation [17] and spatial modulation [18,19] is also reviewed, including generalization to encompass both into a multi-dimensional physical emission structure. Such higher dimension structure may permit enhanced interference avoidance/suppression, particularly when combined with appropriate adaptive processing on receive by exploiting the increased degrees of freedom.

II. POLYPHASE-CODED FM (PCFM)

The implementation of PCFM waveforms is achieved through a modification to the CPM structure [16] that has been used for aeronautical telemetry, deep space communications, and the Bluetooth[TM] wireless standard. For a pulsed radar emission [6], a train of N consecutive impulses with time separation T_p are formed such that the total pulsewidth is $T = NT_p$. The nth impulse is weighted by α_n, the phase change between successive chips of the polyphase code is determined by

$$\alpha_n = \begin{cases} \tilde{\alpha}_n & \text{if } |\tilde{\alpha}_n| \leq \pi \\ \tilde{\alpha}_n - 2\pi \, \text{sgn}(\tilde{\alpha}_n) & \text{if } |\tilde{\alpha}_n| > \pi \end{cases}, \tag{1}$$

where $\tilde{\alpha}_n = \theta_n - \theta_{n-1}$ for $n = 1, \cdots, N$, sgn($\bullet$) is the sign operation, and θ_n is the phase value of the nth chip in the length $N+1$ polyphase code. The stipulations on the shaping filter $g(t)$ are 1) that it integrates to unity over the real line; and 2) that it has time support on $[0, T_p]$. For example, rectangular filter meets these requirements (as do others). The sequence of phase changes are collected into the vector $\mathbf{x} = [\alpha_1 \quad \alpha_2 \quad \cdots \quad \alpha_N]^T$ to parameterize the complex baseband PCFM waveform as [6]

$$s(t;\mathbf{x}) = \exp\left\{ j\left(\int_0^t g(\tau) * \left[\sum_{n=1}^{N} \alpha_n \, \delta\big(\tau - (n-1)T_p\big) \right] d\tau + \theta_0 \right) \right\}, \qquad (2)$$

where θ_0 is the starting phase and $*$ denotes convolution. This waveform provides much greater

spectral containment as shown in Fig. 3 using the same underlying code (a P4 code [2]) as used in
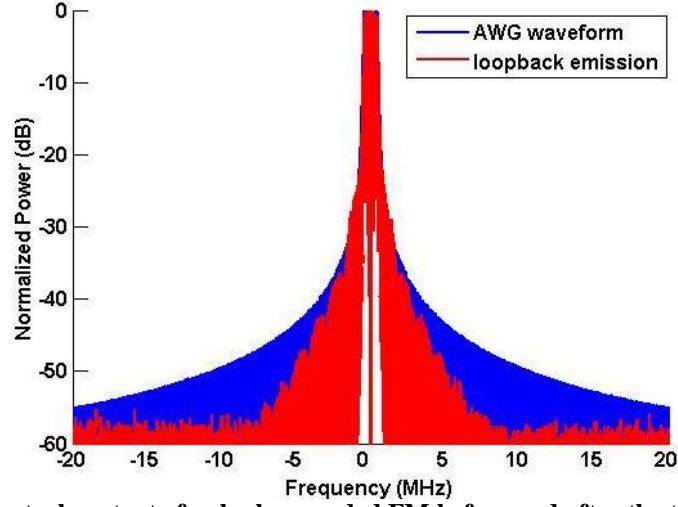
Fig. 2.

Figure 3: Spectral content of polyphase-coded FM before and after the transmitter [6]

Now define $s(t;\mathbf{x}) = T_{\text{PCFM}}\{\mathbf{x}\}$ as the implementation in (2), $u(t;\mathbf{x}) = T_{\text{Tx}}[s(t;\mathbf{x})]$ as the

operation of transmitter distortion upon the waveform to produce the free space emission, and

$\Phi_{(\text{metric})}[u(t;\mathbf{x})]$ as the evaluation of the emission according to some prescribed metric such as

peak sidelobe level (PSL), integrated sidelobe level (ISL), etc. Optimization of the physical

emission [14] can therefore be performed as illustrated in Fig. 4. This physical emission

optimization paradigm can also be readily modified for use with other coding/implementation
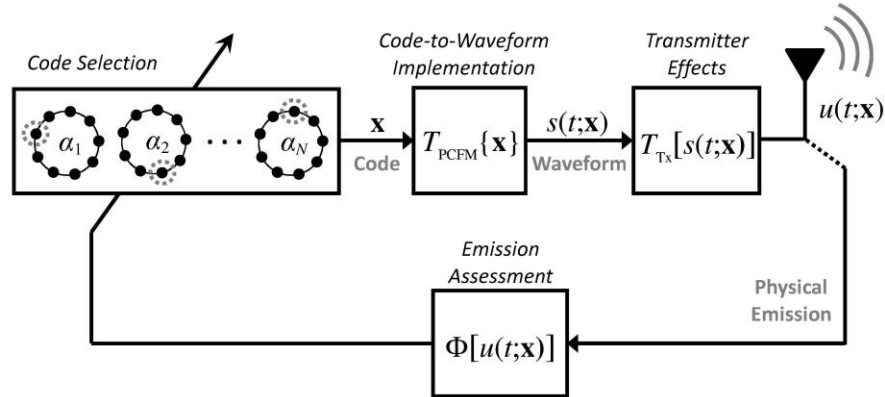
schemes (e.g. OFDM [20]).

Figure 4: Optimization of physical emissions based on PCFM implementation [14]

The "transmitter effects" in Fig. 4 can be realized either with a mathematical model of the transmitter, denoted as Model-in-the-Loop (MiLo) optimization, or with the actual physical transmitter, denoted as Hardware-in-the-Loop (HiLo) optimization. Depending on the computing power available and waveform dimensionality, the MiLo formulation can be performed rather quickly, with the caveat that a model cannot perfectly represent the physical system. In contrast, the HiLo formulation suffers no model mismatch, but the optimization speed is limited by the latencies involved with uploading a waveform, emitting it from the transmitter, and then capturing the emission for evaluation (either in loopback configuration, in an anechoic chamber with separate transmit/receive antennas, or in some other form of controlled measurement arrangement). In [14] examples of loopback optimization and within an anechoic chamber were demonstrated for a solid-state amplifier. Note that unlike *predistortion* techniques (see [21] for an overview) that seek to estimate the parameters of a presumed transmitter model so as to compensate for distortion, the approach in Fig. 4 seeks to incorporate transmitter distortion into the waveform/emission optimization process. As such, the distortion-inclusive design permits incorporation of different transmitter architectures [22] to provide greater freedom in emission design (e.g. [23]) and thus may eventually facilitate joint transmitter/waveform design [24], towards realization of a reconfigurable radar transmitter [25].

The optimization framework in Fig. 4 also implies a search process over the code space of L^N possibilities, where L is the number of possible phase changes. Noting that N closely approximates the waveform time-bandwidth product (BT) and $L \geq 2$, the dimensionality of this search space can clearly be quite large. There are myriad approaches one may take to perform this search [26]. In [14] a greedy search was employed by leveraging the observations that: 1) the range-Doppler ambiguity function of the emission integrates to a constant (i.e. a "conservation of ambiguity"); 2) chirp-like waveforms effectively absorb much of the range-Doppler ambiguity into the well-known range-Doppler ridge; and 3) metrics that are based on attributes of the range-Doppler ambiguity function (such as the zero-Doppler cut, otherwise known as the autocorrelation) are complementary measures of the sidelobe levels. From these observations emerged the *performance diversity* approach [14] that uses a chirp as initialization and alternates between different metrics such as PSL and ISL during a greedy search to help avoid local minima.

Consider an example of waveform optimization when using the mathematical model for the distortion induced by a traveling wave tube (TWT) power amplifier [27]. The injected waveform $s(t; \mathbf{x})$ is first filtered using a 4th order Chebychev filter having a 3-dB passband that is 2.4 times greater than that of the PCFM waveform. This stage is used to model the linear transmitter effects prior to the power amplifier. Denoting the resulting signal that is fed into the TWT as $s_{\text{in}}(t; \mathbf{x})$, the amplified output signal is thus [27]

$$s_{\text{out}}(t; \mathbf{x}) = s_{\text{in}}(t; \mathbf{x}) \, A\big[\, |s_{\text{in}}(t; \mathbf{x})| \,\big] \exp\big\{ j\phi\big[\, |s_{\text{in}}(t; \mathbf{x})| \,\big] \big\} \tag{3}$$

where the terms

$$A[\, r \,] = \frac{1}{1 + \beta_a \, r^2} \quad \text{and} \quad \phi[\, r \,] = \frac{a_\phi \, r^2}{1 + \beta_\phi \, r^2}$$

dictate the degree of amplitude and phase distortion, respectively, for a_ϕ the amplitude-to-phase modulation term, and $\beta_a = \beta_\phi = 1/A_s^2$ for A_s the saturating amplitude.

The time-bandwidth product (*BT*) for this example is $100 \approx N$, for *B* the 3-dB bandwidth. First the PCFM waveform is optimized using the performance diversity approach [14] under the assumption of an idealistic transmitter (no distortion). This optimized FM waveform realizes a PSL of −43.8 dB and an ISL of −26.8 dB. Note that this value of PSL is actually 0.8 dB better than the hyperbolic FM bound [9], which is a useful performance benchmark for constant amplitude FM waveforms.

Two regimes of distortion are then examined using the above model with a_ϕ set to $\pi/12$ per [27] and the value A_s^2 set to 0 dB and −10 dB, representing mild and severe distortion, respectively. Figure 5 illustrates the $A_s^2 = 0$ dB case (mild distortion). Specifically, the distorted waveform has a PSL of −41.4 dB and ISL of −24.9 dB, corresponding to sensitivity losses of 2.4 dB and 1.9 dB, respectively. However, using the TWT model within the optimization process yields a PSL of −42.4 dB and an ISL of −25.0 dB, i.e. a recovery of 1.0 dB and 0.1 dB, respectively.
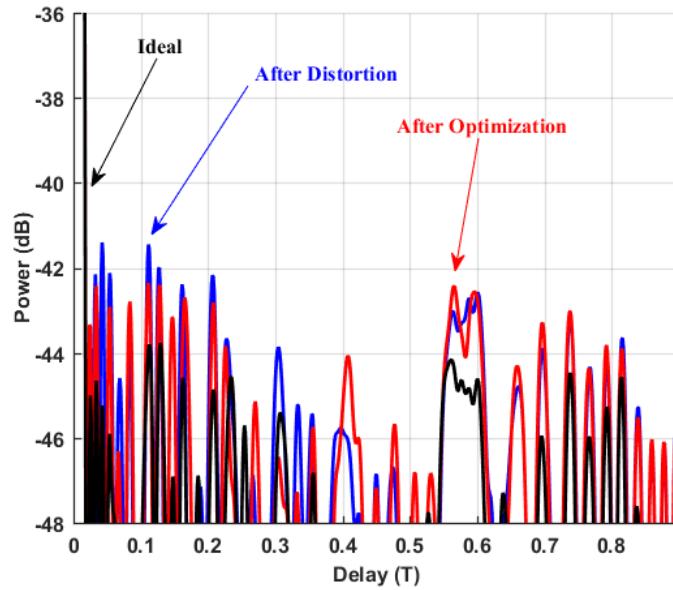
Figure 5: Model-in-the-Loop optimization for a TWT power amplifier (mild distortion)

In contrast, Fig. 6 illustrates the $A_s^2 = -10$ dB case (severe distortion). Now the distorted waveform yields a PSL of -34.2 dB and an ISL of -18.8 dB, corresponding to sensitivity losses of 9.6 dB and 8.0 dB, respectively. When MiLo optimization is applied using the TWT model the resulting PSL attained is -38.8 dB and the ISL is -20.1 dB, i.e. a recovery of 4.6 dB and 1.3 dB of lost sensitivity, respectively.
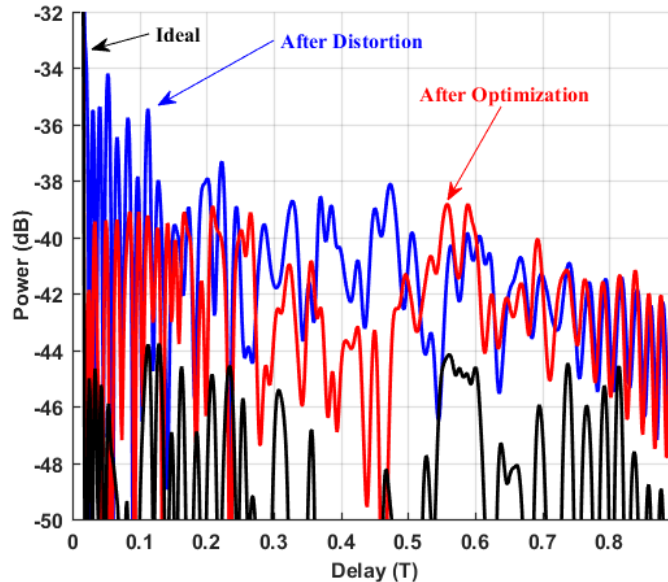
Figure 6: Model-in-the-Loop optimization for a TWT power amplifier (severe distortion)

Clearly, the incorporation of known transmitter distortion effects into the emission optimization can compensate for some, but not all, of the sensitivity loss. However, an appropriate hybridization between MiLo/HiLo optimization and traditional transmitter predistortion [21] could potentially serve as a means to outperform either acting alone. More generally speaking, this holistic perspective also provides the means with which to realize various forms of waveform-diverse emissions in a manner that is physically realizable. Examples of this holistic waveform diversity notion are provided in the next sections.

III. PCFM-BASED POLARIZATION MODULATION

Polarization diversity is widely used in weather radar [28] and synthetic aperture radar (SAR) [29] to improve performance by capturing more information about the sensed environment. The PCFM waveform implementation described in the previous section can be extended to enable fast-time polarization modulation [17] via the incorporation of a hybrid coupler along with an additional waveform. Denoting the two waveforms injected into the input ports of the hybrid coupler as $s_1(t)$ and $s_2(t)$, the resulting emissions from the horizontal (H) and vertical (V) antennas to which the coupler is connected are

$$s_H(t) = \frac{1}{\sqrt{2}}\left(s_2(t) + s_1(t)\right)$$

$$s_V(t) = \frac{1}{\sqrt{2}}\left(s_2(t) - s_1(t)\right)\exp\left(j\kappa\right) \tag{4}$$

where κ is an additional phase term used to select the particular great circle on the Poincaré sphere (Fig. 7) upon which polarization modulation may occur.
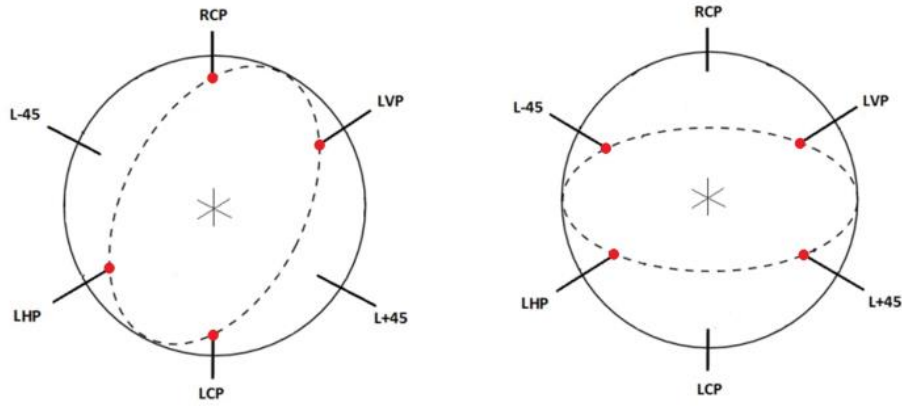

Figure 7: Feasible polarization modulation regions on the Poincaré sphere for (left) $\kappa = 0$ and (right) $\kappa = \pi/2$. RCP: right-hand circular, LCP: left-hand circular, LHP: linear horizontal, LVP: linear vertical, L-45: linear with $-45°$ tilt, L+45: linear with $+45°$ tilt

To control the polarization state in fast-time using the PCFM structure, two length $N+1$ polyphase codes are required. The code $\theta_0, \theta_1, \cdots, \theta_N$ is the same as used in (1) and (2) to construct the length N phase-change sequence $\alpha_1, \alpha_2, \cdots, \alpha_N$ that controls the waveform phase trajectory, noting that $-\pi \leq \theta \leq +\pi$. Denote the second length $N+1$ sequence as $\psi_0, \psi_1, \cdots, \psi_N$, for $-\pi/2 \leq \psi \leq +\pi/2$, which controls the polarization state upon a given great circle of the Poincaré sphere. Defining a polarization state change sequence in the same manner as (1) yields

$$\beta_n = \begin{cases} \tilde{\beta}_n & \text{if } \left|\tilde{\beta}_n\right| \leq \pi/2 \\ \tilde{\beta}_n - \pi\,\text{sgn}\left(\tilde{\beta}_n\right) & \text{if } \left|\tilde{\beta}_n\right| > \pi/2 \end{cases}, \tag{5}$$

where $\tilde{\beta}_n = \psi_n - \psi_{n-1}$ for $n = 1, \cdots, N$.

Collect the polarization state change sequence into the vector $\mathbf{x}_{\mathrm{p}} = [\beta_1 \ \ \beta_2 \ \ \cdots \ \ \beta_N]^T$ and, to avoid confusion, relabel the waveform phase-change vector used in (2) as $\mathbf{x}_{\mathrm{w}} = [\alpha_1 \ \ \alpha_2 \ \ \cdots \ \ \alpha_N]^T$.

Thus, in the same manner as (2), a polarization modulating signal can now be defined as

$$p(t;\mathbf{x}_{\mathrm{p}}) = \exp\left\{ j\left(\int_0^t g(\tau) * \left[\sum_{n=1}^N \beta_n \ \delta\big(\tau - (n-1)T_p\big) \right] d\tau + \psi_0 \right) \right\}. \qquad (6)$$

Fast-time joint waveform/polarization modulation via the hybrid coupler is thus achieved with the waveforms [17]

$$s_1(t;\mathbf{x}_{\mathrm{w}},\mathbf{x}_{\mathrm{p}}) = s(t;\mathbf{x}_{\mathrm{w}})\,p(t;\mathbf{x}_{\mathrm{p}})$$

$$= \exp\left\{ j\left(\int_0^t g(\tau) * \left[\sum_{n=1}^N (\alpha_n + \beta_n) \ \delta\big(\tau - (n-1)T_p\big) \right] d\tau + \theta_0 + \psi_0 \right) \right\}$$

$$. \qquad (7)$$

$$s_2(t;\mathbf{x}_{\mathrm{w}},\mathbf{x}_{\mathrm{p}}) = s(t;\mathbf{x}_{\mathrm{w}})\,p^{-1}(t;\mathbf{x}_{\mathrm{p}})$$

$$= \exp\left\{ j\left(\int_0^t g(\tau) * \left[\sum_{n=1}^N (\alpha_n - \beta_n) \ \delta\big(\tau - (n-1)T_p\big) \right] d\tau + \theta_0 - \psi_0 \right) \right\}$$

Note that the differences between these two waveforms are the phase change sequences $(\alpha_n + \beta_n)$ and $(\alpha_n - \beta_n)$ along with the initial phase values $(\theta_0 + \psi_0)$ and $(\theta_0 - \psi_0)$. When combined in the hybrid coupler via (4) the result is to maintain the desired waveform from (2), overlaid with the desired fast-time polarization modulation. Thus a new physically realizable form of emission control can be achieved. Further details on this emission scheme and associated receive processing can be found in [17].

III. PCFM-BASED JOINT SPATIAL & POLARIZATION MODULATION

The PCFM implementation can also be extended to perform fast-time spatial modulation [18,19] which is a physically realizable form of MIMO radar that is relatively robust to errors induced by mutual coupling [13] and avoids the fluctuations in voltage standing wave ratio (VSWR) that can otherwise occur for MIMO [30]. In [18] and [19] the 1D and 2D instantiations

of spatial modulation were developed, respectively. The inspiration for these schemes is fixational eye movement (FEM) of the human eye, where the "jittering" of the eye has been linked to visual acuity. Thus, such a capability for radar may potentially have application to some form of tracking. Here the notion of spatial modulation is combined with the polarization modulation scheme of the previous section to realize joint Waveform/Spatial/Polarization (WaSP) modulation as a high dimensional emission structure that may permit enhanced interference avoidance/suppression while also facilitating greater information extraction from the sensed environment (particularly when combined with adaptive receive processing).
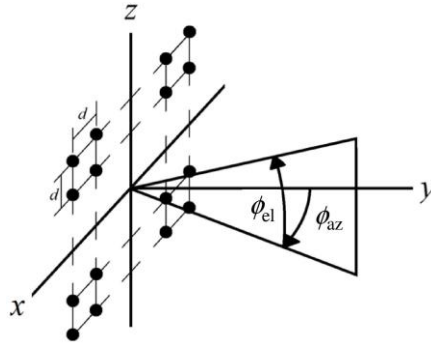

Figure 8: Uniform planar array geometry

Consider a uniform planar array with half-wavelength spacing (Fig. 8) in which, relative to array boresight, azimuth and elevation are measured as the angles ϕ_{az} and ϕ_{el}, respectively. With (0,0) defined as the center of the array, the array elements are indexed as

$$m_x = -(M_x - 1)/2, \ -(M_x - 1)/2 + 1, \ ... \ , (M_x - 1)/2$$

$$m_z = -(M_z - 1)/2, \ -(M_z - 1)/2 + 1, \ ... \ , (M_z - 1)/2$$

(8)

where M_x and M_z are the number of horizontal and vertical array elements, respectively. To perform 2D fast-time spatial modulation, two additional length $N + 1$ codes are needed. Define these codes as $\Delta_{az,0}, \Delta_{az,1}, \cdots, \Delta_{az,N}$ and $\Delta_{el,0}, \Delta_{el,1}, \cdots, \Delta_{el,N}$. Thus, again using the PCFM phase-change framework and making the assumption that the spatial modulation does not "wrap around" the endfire array directions, the spatial phase-change sequences are obtained as [18,19]

$$\varepsilon_{x,n} = \frac{2\pi d}{\lambda}\sin\left(\phi_{az,c}+\Delta_{az,n}\right)\cos\left(\phi_{el,c}+\Delta_{el,n}\right) - \frac{2\pi d}{\lambda}\sin\left(\phi_{az,c}+\Delta_{az,n-1}\right)\cos\left(\phi_{el,c}+\Delta_{el,n-1}\right)$$

$$, \quad (9)$$

$$\varepsilon_{z,n} = \frac{2\pi d}{\lambda}\left[\sin\left(\phi_{el,c}+\Delta_{el,n}\right) - \sin\left(\phi_{el,c}+\Delta_{el,n-1}\right)\right]$$

for $\phi_{az,c}$ and $\phi_{el,c}$ the azimuth and elevation center look directions, respectively.

Collecting the spatial phase-change sequences into the vectors $\mathbf{x}_{s,x} = [\varepsilon_{x,1} \;\; \varepsilon_{x,2} \;\; \cdots \;\; \varepsilon_{x,N}]^T$

and $\mathbf{x}_{s,z} = [\varepsilon_{z,1} \;\; \varepsilon_{z,2} \;\; \cdots \;\; \varepsilon_{z,N}]^T$ then provides the means to realize a spatially modulating signal

using the PCFM structure as [18,19]

$$b_x(t\,;\mathbf{x}_{s,x}) = \exp\left\{-j\left(\int_0^t g(\tau)*\left[\sum_{n=1}^N \varepsilon_{x,n}\,\delta\left(\tau-(n-1)T_p\right)\right]d\tau + \bar{\Delta}_{x,0}\right)\right\}$$

$$, \quad (10)$$

$$b_z(t\,;\mathbf{x}_{s,z}) = \exp\left\{-j\left(\int_0^t g(\tau)*\left[\sum_{n=1}^N \varepsilon_{z,n}\,\delta\left(\tau-(n-1)T_p\right)\right]d\tau + \bar{\Delta}_{z,0}\right)\right\}$$

where $\bar{\Delta}_{x,0} = \frac{2\pi d}{\lambda}\sin\left(\phi_{az,c}+\Delta_{az,0}\right)\cos\left(\phi_{el,c}+\Delta_{el,0}\right)$ and $\bar{\Delta}_{z,0} = \frac{2\pi d}{\lambda}\sin\left(\phi_{el,c}+\Delta_{el,0}\right)$ are the

initial azimuth and elevation modulation phases. Assuming each element location in the $M_x \times M_z$

planar array contains a horizontally polarized element and a vertically polarized element, with

each pair of these horizontal/vertical elements being connected to a hybrid coupler, then the

$2M_x M_z$ driving waveforms are

$$s_{1,m_x,m_z}(t;\mathbf{x}_w,\mathbf{x}_p,\mathbf{x}_{s,x},\mathbf{x}_{s,z}) = s(t;\mathbf{x}_w)\,p(t;\mathbf{x}_p)\,b_x^{m_x}(t\,;\mathbf{x}_{s,x})\,b_z^{m_z}(t\,;\mathbf{x}_{s,z})$$

$$= \exp\left\{j\left(\int_0^t g(\tau)*\left[\sum_{n=1}^N \alpha_n^+(m_x,m_z)\,\delta\left(\tau-(n-1)T_p\right)\right]d\tau + \theta_0^+(m_x,m_z)\right)\right\}$$

$$(11)$$

$$s_{2,m_x,m_z}(t;\mathbf{x}_w,\mathbf{x}_p,\mathbf{x}_{s,x},\mathbf{x}_{s,z}) = s(t;\mathbf{x}_w)\,p^{-1}(t;\mathbf{x}_p)\,b_x^{m_x}(t\,;\mathbf{x}_{s,x})\,b_z^{m_z}(t\,;\mathbf{x}_{s,z})$$

$$= \exp\left\{j\left(\int_0^t g(\tau)*\left[\sum_{n=1}^N \alpha_n^-(m_x,m_z)\,\delta\left(\tau-(n-1)T_p\right)\right]d\tau + \theta_0^-(m_x,m_z)\right)\right\}$$

where

$$\alpha_n^+ (m_x, m_z) = \alpha_n + \beta_n - m_x \varepsilon_{x,n} - m_z \varepsilon_{z,n}$$
$$\theta_0^+ (m_x, m_z) = \theta_0 + \psi_0 - m_x \overline{\Delta}_{x,0} - m_z \overline{\Delta}_{z,0}$$
$$\alpha_n^- (m_x, m_z) = \alpha_n - \beta_n - m_x \varepsilon_{x,n} - m_z \varepsilon_{z,n}$$
$$\theta_0^- (m_x, m_z) = \theta_0 - \psi_0 - m_x \overline{\Delta}_{x,0} - m_z \overline{\Delta}_{z,0}$$

$$(12)$$

according to the element indices m_x and m_z. Note, from (11), that this high-dimensional emission can be decomposed into only four waveforms if the RF hardware permits sufficient freedom in how they can be combined. While the structure in (11) appears to be rather complicated, it is worth noting that the resulting emission from each antenna element is still just an FM waveform, albeit one that is determined from a high-dimensional coding.

Generalizing (4), the signal emitted from the (m_x, m_z) element in the array is

$$s_{H,m_x,m_z}(t) = \frac{1}{\sqrt{2}} \left(s_{2,m_x,m_z}(t) + s_{1,m_x,m_z}(t) \right)$$

$$(13)$$

$$s_{V,m_x,m_z}(t) = \frac{1}{\sqrt{2}} \left(s_{2,m_x,m_z}(t) - s_{1,m_x,m_z}(t) \right) \exp(j\kappa)$$

where all the code dependencies have been suppressed for brevity. Thus the horizontally and vertically polarized far-field emissions are

$$g_H(t, \phi_{az}, \phi_{el}) = \frac{1}{M_x M_z} \sum_{m_x} \sum_{m_z} s_{H,m_x,m_z}(t) e^{j(k_x(\phi_{az},\phi_{el})m_x + k_z(\phi_{el})m_z)}$$

$$,\qquad (14)$$

$$g_V(t, \phi_{az}, \phi_{el}) = \frac{1}{M_x M_z} \sum_{m_x} \sum_{m_z} s_{V,m_x,m_z}(t) e^{j(k_x(\phi_{az},\phi_{el})m_x + k_z(\phi_{el})m_z)}$$

in which $k_x = 2\pi d \sin(\phi_{az}) \cos(\phi_{el}) / \lambda$ and $k_z = 2\pi d \sin(\phi_{el}) / \lambda$, for λ the wavelength of the center frequency. As described in [18] for spatial modulation alone, time-varying and time-aggregated beampatterns can be readily determined for these far-field emissions.

Due to the difficulty with visualizing such a high-dimensional emission, consider the following example in which spatial modulation is performed only in the azimuth direction for $M_x = 10$ dual-polarized elements. The spatial modulation sweeps linearly over an interval of

±11.54° centered on boresight (this interval is first null to first null as defined for a stationary beam). The waveform is a piecewise linear phase approximation to LFM (see [6]) with $BT = 50$. Likewise, the polarization modulation (using κ=0) performs four rotations around the Poincaré sphere during the pulsewidth, beginning at horizontal polarization. This particular great circle corresponds to the left side of Fig. 7 and includes linear horizontal and vertical and left-hand and right-hand circular (and all polarization states in between these).

It is observed in the time-varying beampattern in Fig. 9 that the horizontally and vertically polarized components sweep spatially across the boresight direction during the pulsewidth, while the polarization modulation produces an offset lobing effect between H and V. Figure 10 shows that this particular polarization modulation produces an aggregate beampattern that is nearly identical between H and V, with both revealing the lower broadened peak that arises from spatial modulation [18].

This example demonstrates some of the freedom that is available for emission design as there are numerous different waveform/spatial/polarization modulation combinations that could be realized for all manner of radar modalities. It remains to be seen how different multi-dimensional emission structures can be designed for various sensing applications, though it should be noted that such higher dimensional signal representations are particularly beneficial when combined with adaptive receive processing that can exploit all the degrees of freedom.
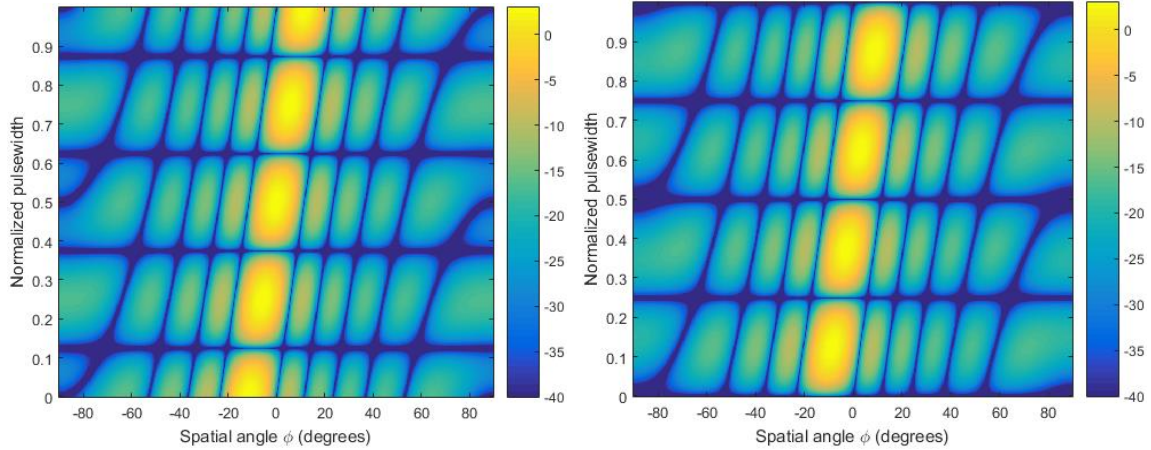
Figure 9: Time-varying beampattern for (left) horizontally polarized and (right) vertically polarized components of a joint Waveform/Spatial/Polarization (WaSP) modulated emission
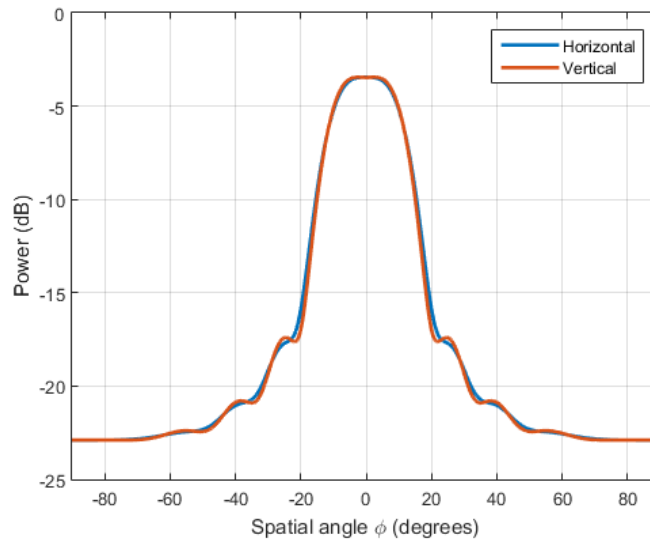

Figure 10: Aggregate beampattern over the pulsewidth for horizontally and vertically polarized components of a joint Waveform/Spatial/Polarization (WaSP) modulated emission

CONCLUSIONS

Recent work leveraging continuous phase modulation (CPM) from communications has enabled the vast array of radar codes previously developed to be physically implemented as polyphase-coded FM (PCFM) waveforms. This implementation permits the inclusion of transmitter distortion effects so as to optimize the physical emission launched from the radar. Further, this formulation allows for generalization to multi-dimensional emissions possessing both spatial and polarization modulation in fast-time over the radar pulsewidth. Ongoing work is

exploring how these emission structures could be incorporated into various sensing modes and prospective benefits (or trade-offs) in so doing.

<u>REFERENCES</u>

[1] M. Vespe, G. Jones, and C.J. Baker, "Lesson for radar: waveform diversity in echolocating mammals," *IEEE Signal Processing Magazine*, vol. 26, no. 1, pp. 65-75, Jan. 2009.

[2] N. Levanon and E. Mozeson, *Radar Signals*, John Wiley & Sons, Inc., Hoboken, NJ, 2004.

[3] H. Griffiths, L. Cohen, S. Watts, E. Mokole, C. Baker, M. Wicks, and S. Blunt, "Radar spectrum engineering and management: technical and regulatory issues," *Proc. IEEE*, vol. 103, no. 1, pp. 85-102, Jan. 2015.

[4] M. Wicks, E. Mokole, S.D. Blunt, V. Amuso, and R. Schneible, *Principles of Waveform Diversity and Design*, SciTech Publishing, 2010.

[5] A.M. Klein and M.T. Fujita, "Detection performance of hard-limited phase-coded signals," *IEEE Trans. AES*, vol. AES-15, no. 6, pp. 795-802, Nov. 1979.

[6] S.D. Blunt, M. Cook, J. Jakabosky, J. de Graaf, and E. Perrins, "Polyphase-coded FM (PCFM) radar waveforms, part I: implementation," *IEEE Trans. Aerospace & Electronic Systems*, vol. 50, no. 3, pp. 2218-2229, July 2014.

[7] C.E. Cook, "A class of nonlinear FM pulse compression signals," *Proc. IEEE*, vol. 52, no. 11, pp. 1369-1371, Nov. 1964.

[8] J.A. Johnston and A.C. Fairhead, "Waveform design and Doppler sensitivity analysis for nonlinear FM chirp pulses," *IEE Proc. F – Communications, Radar & Signal Processing*, vol. 133, no. 2, pp. 163-175, Apr. 1986.

[9] T. Collins and P. Atkins, "Nonlinear frequency modulation chirps for active sonar," *IEE Proc. Radar, Sonar & Navigation*, vol. 146, no. 6, pp. 312-316, Dec. 1999.

[10] I. Gladkova, "Design of frequency modulated waveforms via the Zak transform," *IEEE Trans. Aerospace & Electronic Systems*, vol. 40, no. 1, pp. 355-359, Jan. 2004.

[11] E. De Witte and H.D. Griffiths, "Improved ultra-low range sidelobe pulse compression waveform design," *Electronics Letters*, vol. 40, no. 22, pp. 1448-1450, Oct. 2004.

[12] A.W. Doerry, "Generating nonlinear FM chirp waveforms for radar," *Sandia Report*, SAND2006-5856, Sept. 2006.

[13] G. Babur, P.J. Aubry, F. Le Chevalier, "Antenna coupling effects for space-time radar waveforms: analysis and calibration," *IEEE Trans. Antennas & Propagation*, vol. 62, no. 5, pp. 2572–2586, May 2014.

[14] S.D. Blunt, J. Jakabosky, M. Cook, J. Stiles, S. Seguin, and E.L. Mokole, "Polyphase-coded FM (PCFM) radar waveforms, part II: optimization," *IEEE Trans. Aerospace & Electronic Systems*, vol. 50, no. 3, pp. 2230-2241, July 2014.

[15] D. Henke, P. McCormick, S.D. Blunt, and T. Higgins, "Practical aspects of optimal mismatch filtering and adaptive pulse compression for FM waveforms," *IEEE Intl. Radar Conf.*, Arlington, VA, USA, May 2015.

[16] J.B. Anderson, T. Aulin, and C.-E. Sundberg, *Digital Phase Modulation*, Plenum Press, New York, NY, 1986.

[17] P. McCormick, J. Jakabosky, S.D. Blunt, C. Allen, and B. Himed, "Joint polarization/waveform design and adaptive receive processing," *IEEE Intl. Radar Conf.*, Arlington, VA, USA, May 2015.

[18] S.D. Blunt, P. McCormick, T. Higgins, and M. Rangaswamy, "Physical emission of spatially-modulated radar," *IET Radar, Sonar & Navigation*, vol. 8, no. 12, Dec. 2014.

[19] P. McCormick and S.D. Blunt, "Fast-time 2-D spatial modulation of physical radar emissions," *Intl. Radar Symp.*, Dresden, Germany, June 2015.

[20] J. Jakabosky, L. Ryan, and S.D. Blunt, "Transmitter-in-the-loop optimization of distorted OFDM radar emissions," *IEEE Radar Conference*, Ottawa, Canada, Apr./May, 2013.

[21] F.M. Ghannouchi and O. Hammi, "Behavioral modeling and predistortion," *IEEE Microwave Magazine*, pp. 52-64, Dec. 2009.

[22] F.H. Raab, P. Asbeck, S. Cripps, P.B. Kenington, Z.B. Popovic, N. Pothecary, J.F. Sevic, and N.O. Sokal, "Power amplifiers and transmitters for RF and microwave," *IEEE Trans. Microwave Theory & Techniques*, vol. 50, no. 3, pp. 814-826, Mar. 2002.

[23] L. Ryan, J. Jakabosky, S.D. Blunt, C. Allen, and L. Cohen, "Optimizing polyphase-coded FM waveforms within a LINC transmit architecture," *IEEE Radar Conf.*, Cincinnati, OH, May 2014.

[24] H. Griffiths, S. Blunt, L. Cohen, and L. Savy, "Challenge problems in spectrum engineering and waveform diversity," *IEEE Radar Conf.*, Ottawa, Canada, Apr./May 2013.

[25] M. Fellows, M. Flachsbart, J. Barlow, J. Barkate, C. Baylis, L. Cohen, R.J. Marks, "Optimization of power-amplifier load impedance and waveform bandwidth for real-time reconfigurable radar," *IEEE Trans. Aerospace & Electronic Systems*, vol. 51, no. 3, pp. 1961-1971, July 2015.

[26] C. Blum and A. Roli, "Metaheuristics in combinatorial optimization: overview and conceptual comparison," *ACM Computing Surveys*, vol. 35, no. 3, pp. 268-308, Sept. 2003.

[27] E. Costa, M. Midrio, and S. Pupolin, "Impact of amplifier nonlinearities on OFDM transmission system performance," *IEEE Communications Letters,* vol. 3, no. 2, pp. 37-39, Feb. 1999.

[28] V.N. Bringi and V. Chandrasekar, *Polarimetric Doppler Weather Radar: Principles and Applications*, Cambridge, U.K.: Cambridge Univ. Press, 2001.

[29] J.J. van Zyl and Y. Kim, *Synthetic Aperture Radar Polarimetry*, John Wiley & Sons, Inc., Nov. 2011.

[30] Daum, F., Huang, J., "MIMO radar: snake oil or good idea?" *IEEE AES Mag.*, May 2009.